Sensitivity and Scattering in a Monolithic Heterodyned Laser Biochemical Sensor

Daniel A. Cohen, Jill A. Nolde, Anna Tauke Pedretti, *Student Member, IEEE*, Chad S. Wang, *Student Member, IEEE*, Erik J. Skogen, and Larry A. Coldren, *Fellow, IEEE*

***Abstract*—We discuss the sensitivity of a novel biochemical sensor based on the heterodyne detection of the optical frequency shift between two monolithically integrated frequency-tunable lasers. A hundred-fold improvement may be obtained by replacing the traditional ridge waveguide structure with a quasisymmetrically clad channel waveguide, which we demonstrate in a simple coupled-cavity sensor. In most cases, the optical scattering from biomolecules bound to such a waveguide will be negligible.**

***Index Terms*—Biomedical measurements, integrated optoelectronics, semiconductor lasers, sensors.**

I. Introduction

THERE is a growing need for biochemical sensors that are sensitive, fast, small, low-powered, and inexpensive, for use in medical, industrial, and military applications. Optical techniques based on absorption spectroscopy, Raman scattering, fluorescence, and surface plasmon resonance are the most sensitive for biochemical detection, and some of these approaches have been commercialized [1], [2]. However, attempts to adapt these laboratory techniques to the microscale have suffered by not integrating the light source with the sensor. A number of interferometric sensors have been demonstrated utilizing integrated optics in conjunction with an off-chip laser [3], [4]. Refractive index changes as low as $5 \cdot 10^{-8}$ have been detected in bulk fluids, using an interaction length of 4 mm [5]. These sensors may serve well for industrial or environmental monitoring where sample sizes are large, but they are inappropriate for biological monitoring where samples sizes of a picoliter, delivered by microfluidic means are common. Sensors have also been demonstrated utilizing diode lasers monolithically integrated with Mach–Zehnder interferometers [6]. The results are encouraging, and suggest a promising new market for photonic integrated circuits. We have recently reported chemical sensing with a monolithically integrated device comprising a pair of sampled-grating distributed Bragg reflector (SGDBR) lasers, a field combiner, and a photodiode [7]. We called this device a tunable laser cavity sensor (TLCS). To achieve high sensitivity and dynamic range, a different set of parameters must be optimized than would be the case for traditional diode laser applications. For example, modulation speed and output power are nearly irrelevant here, while wavelength tuning and linewidth remain important. New criteria arise, such as mode penetration out of the waveguide, and the resulting increase in scattering loss. In this paper, we review the experimental results and discuss the design issues affecting sensitivity of this fully integrated evanescent field sensor. Some of the issues apply equally well to the integrated interferometers.

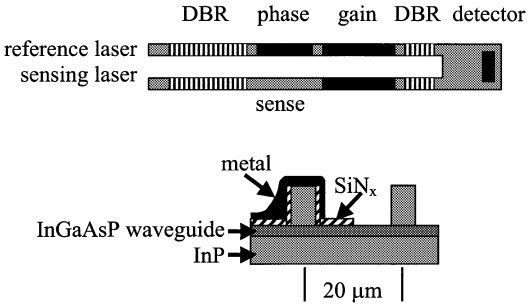

Fig. 1. Schematic of the tunable laser cavity sensor (TLCS). Changes in the refractive index of the medium surrounding the sensing laser's ridge waveguide induce a shift in the laser's optical frequency, detected by heterodyne mixing with an on-chip frequency-tunable reference laser. Lower figure shows a cross-section of the phase/sensing region.

As shown in Fig. 1, the device consists of a pair of frequency-tunable lasers that emit into a slab waveguide field combiner. Embedded within the slab, at the point where the two diffracting fields overlap, is a photodetector. The overlapping fields produce a heterodyne signal equal in frequency to the difference between the optical frequencies of the two lasers. A portion of one laser's passive waveguide is left exposed to the analyte. This laser's evanescent field then overlaps with the surrounding medium such that a small shift in the surrounding index of refraction induces a shift in optical frequency, and a corresponding shift in the heterodyne frequency. This index shift may be due to contamination in a bulk fluid, binding of an antigen to an antibody immobilized on the waveguide surface, or similar binding between DNA fragments and complimentary strands bound to the waveguide. The latter two applications rely on selective chemistry at the surface to bind only the target molecule or pathogen. Since the evanescent field decays within tens of nanometers from the surface, the device is insensitive to unbound species. Elements of this approach have been demonstrated elsewhere, using fiber external cavity lasers with diode gain sections [8], [9]. However, these demonstrations were neither compact nor robust by microelectronic standards.

Manuscript received February 15, 2003; revised July 10, 2003. This work was supported by the Defense Advanced Research Projects Agency within the Bioflips and Simbiosys Programs under Contract DAAD 19-00-1-0400 and Contract F30602-01-2-0538.

The authors are with the Department of Electrical and Computer Engineering, University of California, Santa Barbara, CA 93106 USA (e-mail: cohen@ece.ucsb.edu).

Digital Object Identifier 10.1109/JSTQE.2003.819481

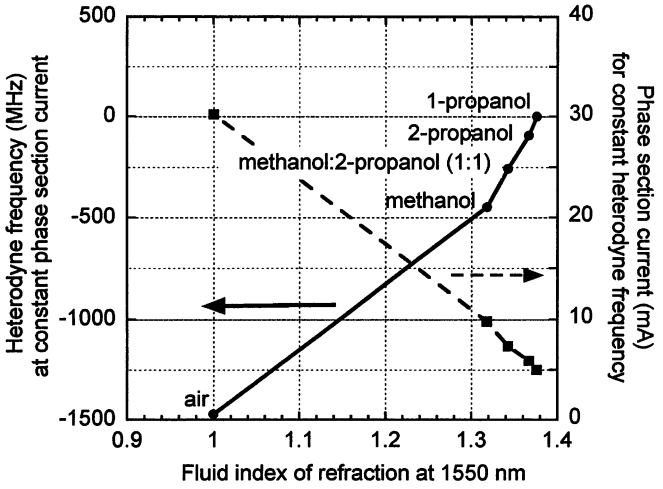

Fig. 2. Sensing bulk fluids with the TLCS. A frequency precision of 1 MHz yields a bulk index resolution of $1 \cdot 10^{-4}$. The sensor may operate open loop with a fixed reference laser frequency, or closed loop with a fixed heterodyne frequency. The SGDBR reference laser provides 5-THz tuning for wide dynamic range.

The shift in heterodyne frequency, Δf, is given by

$$\frac{\Delta f}{f} = \Gamma \frac{\Delta n}{n} \tag{1}$$

where f is the optical frequency, Δn is the change in refractive index in the region of the evanescent field, n is the effective modal index averaged over the entire cavity, and Γ is the fraction of the sensing laser's optical energy that resides in the exposed evanescent field. The high sensitivity of this technique originates from the relative precision with which the frequency may be measured: based on the linewidth of individual SGDBR lasers, we expect a heterodyne linewidth of 10 MHz. With simple processing a frequency shift of only 1 MHz should be detectable, while the optical frequency is 200 THz. Thus, the sensor should detect a fractional shift in the *modal* index of only $5 \cdot 10^{-9}$. If the mode overlap with the analyte is 1%, and the laser modal index is 3.3, this corresponds to an absolute shift in the analyte's index of less than $2 \cdot 10^{-6}$.

II. Tunable Laser Cavity Sensor Results

A. Description of the Device

The SGDBR lasers have been described in detail elsewhere [10]. We mention here that they consist of a 350-nm-thick GaInAsP waveguide layer, clad by InP. Seven compressively strained quantum wells are grown above the waveguide, and are etched away prior to MOCVD regrowth, to form passive waveguide regions. The quantum wells are left intact to form the detector. A ridge waveguide structure is used, with a nominal ridge width of 2.5 μm, etched chemically down to the top quantum well barrier in the active region, or to the top of the waveguide in the passive regions. The two laser ridges are 20 μm apart, and terminate in a common slab waveguide 23 μm wide. Imbedded in the slab, approximately 200 μm from the input end is the photodetector. The sampled DBR mirrors and the phase adjustment region in the reference laser are tuned by current injection. The corresponding phase adjustment region of the sensing laser is left without contact or dielectric layers, so that the evanescent field from the waveguide can interact with the surrounding medium.

B. Experimental Details

The sensor was tested in an open reservoir containing one of five different fluids, including air. Alcohol mixtures were used instead of aqueous or aromatic solvents, to avoid excessive bubbling due to electrolysis at the contacts, and to insure clean exchange of fluids. The reservoir, in turn, rested upon a temperature-controlled stage. The optical signal from the back facets of the two lasers was coupled through single-mode fiber to a high-resolution optical spectrum analyzer, used as an independent measure of wavelength shift. The device was biased with dc electrical probes, and the microwave signal from the photodetector was coupled by way of a coplanar waveguide probe to an electrical spectrum analyzer, without amplification. Fluids were exchanged by pipette.

C. Bulk Sensing Results

The heterodyne frequency shifted approximately linearly with the index of refraction of the fluid, as shown in Fig. 2. Indeed, the linearity was quite good, except when exchanging the fluid to air. This is probably the result of a significant change in the field profile when the surrounding index changed from approximately 1.3–1.0. Also shown is the tuning current supplied to the reference laser's phase section, to maintain a fixed heterodyne frequency. This feedback technique provides a very wide dynamic range without the need for an integrated high-speed detector, because the SGDBR laser is tunable over 5 THz. It also allows the use of narrow band electrical filters for an improved signal-to-noise ratio.

At 1550 nm, the index difference between 1-propanol and 2-propanol is 0.009. The heterodyne signal shifted 93 MHz when these two fluids were exchanged. The modal index of this ridge structure is 3.3, so from (1) we calculate the experimental mode overlap with all of the surrounding fluid to be $1.8 \cdot 10^{-4}$. The sensing region occupied 40% of the total cavity length, that is $\Gamma_z = \Gamma / \Gamma_{xy} = 0.4$, so that $\Gamma_{xy} = 4.4 \cdot 10^{-4}$.

D. Linewidth

The heterodyne linewidth (FWHM) is shown as a function of photocurrent in Fig. 3. As expected, the linewidth decreases inversely with power, and reaches 15 MHz at a few milliamps. Further reduction in the linewidth was hampered by electrical noise from the computer controlled current sources, and the probing arrangement. We note that SGDBR lasers with a short-term linewidth below 5 MHz are available commercially [11], so that with a packaged device and low noise current sources we can expect a heterodyne linewidth of twice this or 10 MHz. The ability to signal-average to obtain a more precise measure of the frequency depends on the temperature stability of the device, discussed next.

E. Temperature Sensitivity

The optical frequency of an SGDBR laser drifts with temperature at 13–15 GHz/°C, as does any single frequency diode laser

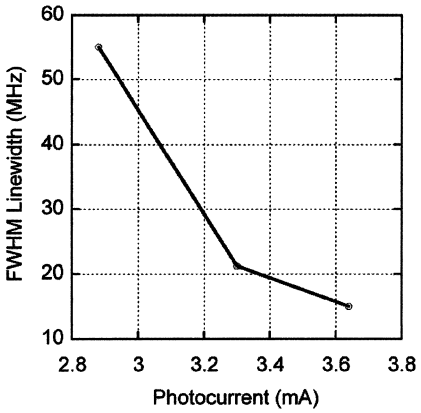

Fig. 3. FWHM, obtained with a probed device and computer controlled current sources. Commercial SGDBR lasers with filtered current sources yield 5-MHz linewidths. Photocurrent includes 0.8-mA dark current. Heterodyne frequency held at approximately 1 GHz.

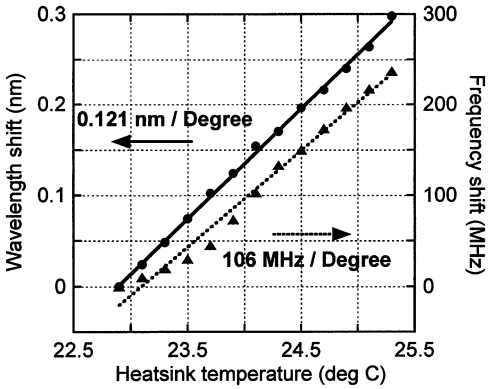

Fig. 4. Wavelength shift of the individual lasers, and frequency shift of the heterodyne signal, in response to changes of the heatsink temperature. 0.121 nm/°C corresponds to 15 GHz/°C.

at this wavelength. However, since the heterodyne frequency is the difference between two nominally identical lasers, it should be orders of magnitude more stable than the individual lasers. We tested this by varying the heatsink temperature below the TLCS. As shown in Fig. 4, the signal drift was 106 MHz/°C, less than 1% of the drift of the individual lasers. The residual drift arises because the two lasers may have slightly different scattering or absorption losses, and thus operate at slightly different carrier densities. The absorption losses, in particular, depend on the tuning currents applied to the phase and mirror sections, so the temperature sensitivity will be influenced by the current needed to align the two lasers' frequencies. In principle, additional loss could be added to one laser to better match the operating point of the other laser. Alternatively, a reference pair of lasers, neither of which has an exposed sensing region, may be used as an on-chip temperature monitor. In this case, increasing the difference in loss between the two lasers in the reference pair will increase the temperature sensitivity, as desired for a temperature monitor.

With the present temperature sensitivity, a substrate temperature drift of 10 mK would produce a 1-MHz error in the heterodyne frequency, comparable to the anticipated frequency resolution. For clinical applications, thermoelectric temperature controllers are commercially available with 5-mK stability. For many portable or cost-sensitive applications, however, the sensor must operate unstabilized. In this case, we can use the known temperature response in conjunction with an on-chip temperature measurement (perhaps from a reference pair as above), to interpret the heterodyne signal. We note that the 35-nm tuning range of the SGDBR lasers will allow nulling the heterodyne signal over the lasers' entire 80 °C operating range.

The InP sensor is flip-chip bonded to a silicon microfluidic circuit for sample delivery, so we must consider the thermal effects of the fluid. In many applications, after a 1-ml sample is pumped or wicked into the sensor, it will remain static for the duration of the assay. The small volume and the intimate contact with the silicon channel insure that the fluid will reach thermal equilibrium within seconds, whereas an affinity assay will generally require a minute or more to complete. The transient frequency shift due to introduction of the sample will be easy to discern. In continuous flow assays, with a flow rate of 10 ml/min, the fluid will again reach substrate temperature after traversing a few millimeters of the silicon channel. To insure this, a compact serpentine channel can be used, upstream of the sensor.

Since the lasers generate heat, there will be a temperature gradient in the fluid. A static gradient merely causes a static frequency offset that can easily be nulled out. A varying gradient, however, due perhaps to varying DBR tuning currents, will produce a spurious signal. To the extent the fluid properties and flow rate are known, this effect is predictable and can be compensated. Alternatively, a pair of reference lasers can be used as a temperature monitor, as previously described.

III. Sensitivity Analysis

A. Mode Penetration From the Ridge Waveguide

Equation (1) shows that the key to achieving high sensitivity in the TLCS is to obtain a high overlap between the optical mode and the region to be sensed. In Fig. 5(a), we show the calculated optical field profile in the ridge waveguide structure of the sensing region. The only field penetration out of the waveguide occurs in the corners between the ridge and the waveguide layer, and the calculated mode overlap with all of the bulk fluid outside the waveguide is only 0.04%, in good agreement with our experimental result. We cannot simply thin the upper cladding to increase the overlap, because the big difference between the waveguide index and the surrounding medium forces the optical mode deep into the semiconductor. Indeed, as the upper cladding is thinned toward zero, the asymmetry cuts off propagation [12].

B. Mode Overlap With Thin Analytes

There is no cutoff of the lowest order optical mode in a symmetrically clad waveguide. Thus, if we replace the lower cladding in the structure with a material of low index of refraction, approximately matching the index of refraction of the analyte, we should be able to thin the waveguide thickness and dramatically increase the mode overlap with the analyte. It has also been pointed out that to obtain high sensitivity to thin layers on the waveguide surface, such as used in affinity assays, a big difference between the core and cladding indices is

needed, along with a thin core [13]. This was demonstrated with dielectric waveguides such as Si_3N_4/SiO_2 or TiO_2/SiO_2, which were considered high contrast with an index ratio of 2.2/1.5. In the case of semiconductor waveguides, even the "high" index dielectrics behave as low-index cladding. In Fig. 5(b), we show the mode profile for a quasisymmetrically clad channel waveguide formed between a GaInAsP core $(\mathrm{n} = 3.452)$, a Si_3N_4 lower cladding $(\mathrm{n} = 2.0)$, and an aqueous upper cladding $(\mathrm{n} = 1.33)$. In comparison to Fig. 5(a), the mode profile is concentrated and symmetric, with significant energy in the evanescent field immediately next to the waveguide. In this case, the calculated mode overlap with a 10-nm-thick antigen layer, bound to the top surface by a 10-nm-thick antibody layer, is above 1%, two orders of magnitude greater than the original ridge waveguide design.

C. Symmetrically Clad Designs

Fig. 6 shows the mode overlap with a 10-nm-thick biomolecule layer, separated from the waveguide by a 10-nm-thick binding layer, for different lower cladding materials and assuming an aqueous upper cladding. We assume that both the antibodies and antigens have an index of refraction of 1.48 [3]. Since we wish to use the same waveguide in the active section of the laser, we also show the mode confinement in the quantum wells as a function of waveguide thickness. As can be seen, with an InP lower cladding, the waveguide layer cannot be thinned below 300 nm before the mode is forced deep into the lower cladding and approaches cutoff. On the other hand, a lower cladding index as high as 2 allows the waveguide core to be thinned below 100 nm, with a resulting mode overlap with the target molecule nearly as high as for the truly symmetric case. The peak in the symmetric case occurs because below 70 nm the optical mode begins to expand. Thus, a wide variety of dielectric materials may be used as quasisymmetric lower cladding layers that lead to a hundred-fold increase in sensitivity over the InP-clad design.

D. Index Increment, Sensitivity, and Nanoparticle Enhanced Assays

Fig. 6 gives the mode overlap with a hypothetical uniform film of molecules bound to the waveguide surface. To calculate the sensitivity of the TLCS in the case of low-level detection, we need to know the shift in modal index due to binding of sparsely distributed particles of finite size. The change in refractive index of a fluid due to the uniform dispersion of N particles per unit volume is given by [14]

$$\Delta n = \frac{3}{2}\left(\frac{n'^2 - 1}{n'^2 + 2}\right) NV \tag{2}$$

where n' is the ratio of the index of the particle to the index of the pure fluid, and V is the volume of the spherical particle. The product NV is just the fraction of space occupied by the particles. When the optical field is a waveguide mode, we must multiply by Γ_{xy} to account for limited overlap between the optical field and the particles. We also use the mode volume, V_{mode}, to

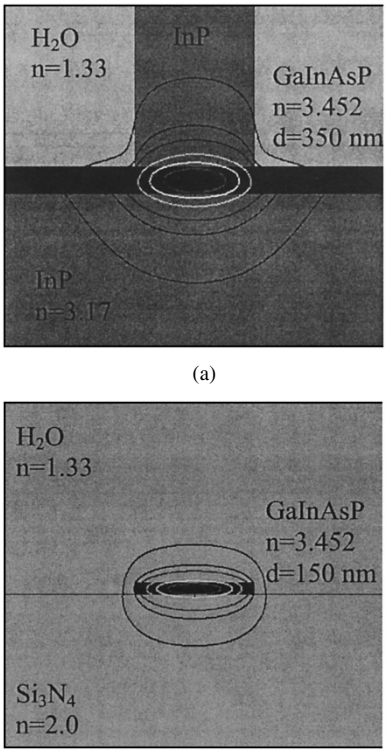

Fig. 5. Optical field contours, displayed at 1%, 10%, 20%, 40%, 60%, and 80% of maximum field amplitude. (a) Very little field penetrates out of the high index semiconductor in the ridge structure used in the demonstrated TLCS. (b) Quasi-symmetrically clad waveguide allows a thinner high index core, providing a higher mode overlap with thin layers adjacent to the waveguide.

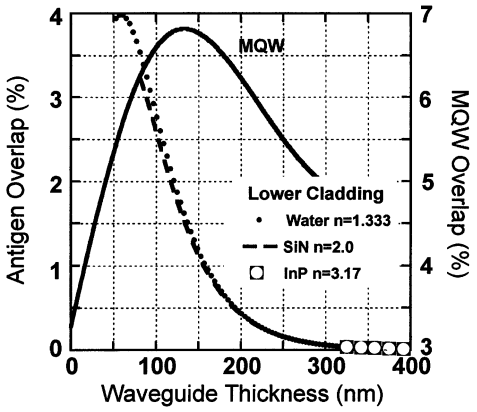

Fig. 6. Mode overlap with a thin antigen layer, and with the MQW gain region. The asymmetry between InP cladding on one side of the waveguide and water on the other side cuts off propagation in waveguides less than 300-nm-thick.

calculate N, noting that the mode confinement in the waveguide core, $V_{\mathrm{mode}} = V_{\mathrm{core}}/\Gamma_{\mathrm{core}}$ [12]

$$N = N^{\#}\frac{\Gamma_{\mathrm{core}}}{V_{\mathrm{core}}} \tag{3}$$

where $N^{\#}$ is the number of particles on the surface (a pure number). For particles of radius a, we estimate the mode overlap Γ_{xy} by calculating the optical intensity at the center of the particle and multiplying by the particle area. This is equivalent to

assuming that the evanescent field decay is approximately linear over the dimension of the particle. Then

$$\Delta n = \frac{3}{2}\left(\frac{n'^2-1}{n'^2+2}\right)\Gamma_{xy}N^{\#}\frac{\Gamma_{\text{core}}}{V_{\text{core}}}\left(\frac{4}{3}\pi a^3\right). \quad (4)$$

While Fig. 6 shows that the mode overlap with a thin antigen layer peaks at a waveguide thickness of 70 nm, this thin waveguide may be very difficult to fabricate. Instead, we assume a more conservative waveguide thickness of 150 nm, which gives a good overlap with both the antigen layer and the MQW active region. In Fig. 7, we show the change in modal index as a function of the number of particles bound to a waveguide of dimensions 0.15 μm $\times$ 2 μm $\times$ 1000 μm. We use the particle radius as a second parameter, assume the particle index of refraction is 1.57 representative of polystyrene nanoparticles (and approximately correct for proteins) and assume that the surrounding medium is water with index 1.33. The curves terminate at the close-packed number given by $(\text{waveguide length} \times \text{waveguide width})/(\text{particle diameter}^2)$.

Also shown in Fig. 7 is the sensitivity limit of the TLCS, assuming a frequency precision of 1 MHz. We see that for protein antigens 5 nm in radius, $2 \cdot 10^5$ copies must be bound. This corresponds to about 150 femtograms of material. For macromolecules or pathogens larger than 50 nm in radius, single copies should be detectable.

A number of authors have used polystyrene beads bound to the target antigens to enhance the sensitivity of refractometric measurements [15]. This is particularly useful when the target is a small molecule such as a drug. A thousand-fold improvement in sensitivity has been reported, easily understood by reference to Fig. 7. If the low index polystyrene is replaced by a high-index semiconductor nanoparticle such as silicon, (2) shows that the sensitivity may be further improved by a factor of five.

E. Fabrication

In the experimental version of the TLCS, the sensing region waveguide was identical to that used in the active region, so the reflections and scattering loss at the transition were negligible. We have shown that to obtain high sensitivity, the waveguide core should be thinned to less than 150 nm, and the InP lower cladding must be replaced with a low-index material. We have not discussed the many possible fabrication techniques for such a structure, or the difficulties in the transition between the active and sensing regions. We suggest that the lower cladding may be replaced by selective wet etching followed by deposition of a polymer cladding, or by bonding the device upside down to a superstrate and etching away the growth substrate. Alternatively, aluminum-bearing materials might be used in the cladding, allowing oxidation or selective etching or both. We chose the oxidation method to demonstrate the feasibility of incorporating a quasisymmetrically clad waveguide with a normal laser structure, as we next describe briefly. Full details of the performance will be reported separately.

We built a coupled-cavity laser sensor in the GaAs material system, as shown schematically in Fig. 8. The active region consisted of three 8-nm InGaAs wells with 8-nm GaAs barriers, located above a 200 nm thick waveguide core composed of $Al_{0.2}Ga_{0.8}As$. A passive section was formed by dry etching through the quantum wells to the waveguide core. A second dry etch was then used to define a ridge structure that narrowed from 6 μm in the gain and absorber sections to 3 μm in the sensing region, and penetrated through a 300-nm-thick $Al_{0.98}Ga_{0.02}As$ layer beneath the waveguide core. Wet oxidation was then used to convert this $Al_{0.98}Ga_{0.02}As$ layer to an oxide layer with a refractive index of approximately 1.6. The oxidation was timed to completely convert the material below the narrow sensing region but leave an unoxidized width of approximately 3 μm below the active and absorber waveguides. This self-aligned process left a high-index-contrast quasisymmetrically clad waveguide coupled to a more conventional laser waveguide. The gain, sense, and absorber sections were 400-, 40-, and 200-μm-long, respectively. The process was completed with Ti/Pt/Au p-contacts, and AuGe/Ni/Au n-contacts on the back of the thinned substrate.

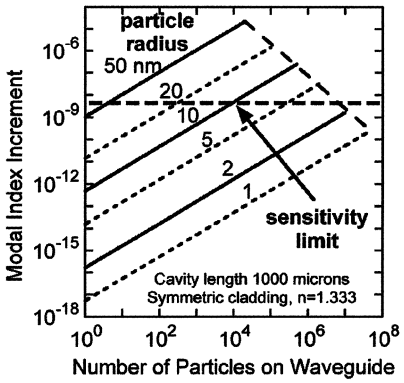

Fig. 7. Modal index increment due to binding particles on the waveguide surface. The sensitivity limit, based on an assumed frequency precision of 1 MHz, is shown. Antigens of interest range from 1 nm to several micrometers in diameter.

The cleave at the front (gain) end, the etched facet at the interface between the gain and sensing regions, and the etched facet at the interface between the sensing and absorber regions formed a three mirror cavity. In operation, the absorber region was grounded so that no light returned from the rear cleaved facet. The net reflectivity from the two etched facets was modulated by the resonance in the passive cavity, producing a mode filter whose center wavelength depended on the modal index of refraction in the passive section. This, in turn, was influenced by the evanescent interaction with the medium surrounding the passive waveguide.

To quantify this evanescent interaction, the entire device was submerged in a temperature-controlled bath of fluid held at 18 °C. To avoid wavelength shifts due to self-heating, the device was tested with 500-ns pulses at a repetition rate of 10 kHz. Five different alcohol mixtures were tested; for clarity, only three of the lasing spectra are shown in Fig. 9. For each spectrum, an interpolation scheme was used to determine the filter center wavelength from the intensities of the three strongest lasing modes. We found that the filter wavelength, λ_f, shifted nearly linearly with the index of refraction of the bathing fluid, with

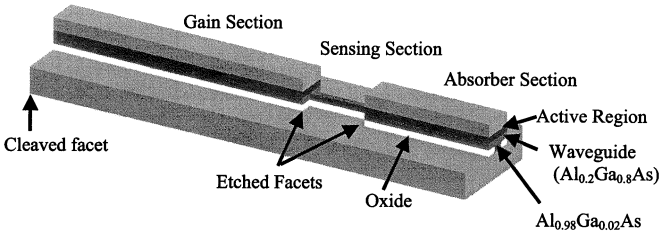

Fig. 8. Schematic of the layer and device structure of the coupled cavity laser sensor. Note the narrower ridge width in the sensing region, allowing complete oxidation beneath the waveguide layer to form a quasisymmetrically clad waveguide.

$\mathrm{d}\lambda_f/\mathrm{d}n = 13.5$ nm. Similarly to (1), the modal overlap with the fluid to be sensed is given by

$$\frac{\Delta\lambda_f}{\lambda_f} = \Gamma\frac{\Delta n}{n}.$$

Note that this describes the passive cavity resonance, not the total cavity resonance, so that $\Gamma_z = 1$ and $\Gamma = \Gamma_{xy}$. From the data, Γ_{xy} was calculated to be 4.8%, in fair agreement with a two-dimensional (2-D) mode simulation of 3.7%. The discrepancy may be due to poor knowledge of the true oxide index of refraction. This is a hundred-fold improvement over the asymmetric ridge waveguide result.

Oxidation cannot be used in the InP material system in which we have fabricated the SGDBR-based sensor, but selective wet etching can be used [16], [17]. Thus, we should be able to incorporate the quasisymmetrically clad sensing waveguide into the InP-based TLCS.

While the coupled-cavity laser sensor depended on a reflection at the interface between the active and sensing waveguides, such a reflection would make a SGDBR laser difficult to control. To avoid such problems, angled interfaces and waveguide tapers have been utilized in SGDBR-based photonic integrated circuits to suppress reflections from cleaved facets [18]. Inasmuch as the impedance discontinuity and mode mismatch at a transition between the asymmetric and symmetric waveguides is smaller than at the transition from an asymmetric waveguide to free space, these measures should be effective between the active and sensing waveguides as well. We point out that since this is an in-plane device, there is enough gain available to overcome the loss at such an angled interface. We do not make light of the work needed to develop these low-reflection transitions, but believe that the demonstrated benefits justify the effort.

IV. Scattering and Absorption

If the mode overlap with particles on the waveguide surface is made large, the sensor might also suffer a significant increase in optical scattering loss. To evaluate this potential problem, we adapt Rayleigh scattering theory [14]. The scattering cross section C_{sca} is the total power scattered by a particle dP, normalized by the incident intensity at the particle

$$C_{\mathrm{sca}} = dP/\left(\Gamma_{xy}P_0/\pi a^2\right). \tag{5}$$

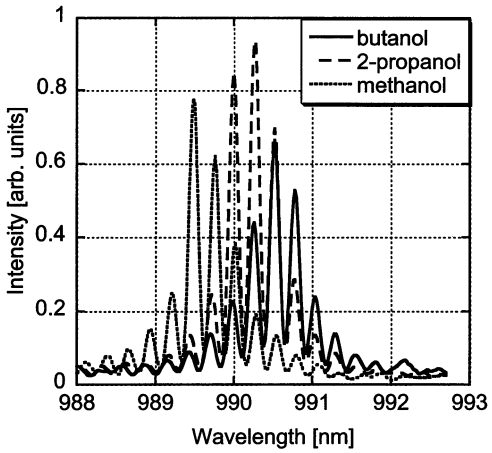

Fig. 9. Lasing spectra for three different fluids bathing the sensor. The mode filter center wavelength depends on the fluid index of refraction, and is found by interpolation between the dominant modes.

Let N_A be the surface density of identical particles on the waveguide of width w. Upon traversing length dz, the optical field will suffer a loss

$$\frac{dP}{P_0} = -N_A w\, dz \Gamma_{xy}\frac{C_{\mathrm{sca}}}{\pi a^2}. \tag{6}$$

Rearranging to obtain an expression for dP/dz, and solving the differential equation yields

$$P(z) = P_0 \exp\left[-N_A w \Gamma_{xy}\frac{C_{\mathrm{sca}}}{\pi a^2} z\right]. \tag{7}$$

Inserting the scattering cross section of a small spherical particle ($a \ll \lambda$) [14], and identifying the exponential decay term as the modal loss $\langle\alpha\rangle$, we arrive at

$$\langle\alpha\rangle = -N_A w \Gamma_{xy}\frac{128}{3}\pi^4\left(\frac{a}{\lambda}\right)^4\left(\frac{n'^2-1}{n'^2+2}\right)^2. \tag{8}$$

The dependence on $(a/\lambda)^4$ limits the scattering loss in the TLCS, which operates at 1550 nm. Indeed, for proteins or polystyrene particles, the loss remains below 1 cm^{-1} even up to the close-packed surface density. Note that the dependence on the relative index is stronger for scattering than for the index increment. If high-index particles are used for sensitivity enhancement, the scattering loss increases faster. Nonetheless, even for silicon particles the scattering does not become significant until the particle radius exceeds 20 nm and the particle density approaches the close packed limit, as Fig. 10 shows. We point out that Rayleigh scattering assumes that the particles are sufficiently isolated so that phase coherence between scatterers may be ignored. This is clearly not valid in the close-packed limit, at which point a coupled-mode analysis may be more appropriate. In any case, the only instance relevant to sensing in which the scattering may be a problem is for a nanoparticle-enhanced flow assay, in which the enhancing particles are packed closely on the waveguide, and released upon binding of an untagged antigen [19], [20].

We might also ask whether the increased field penetration out of the sensing waveguide can lead to significant absorption loss. In most chemical or biological materials, the absorption in

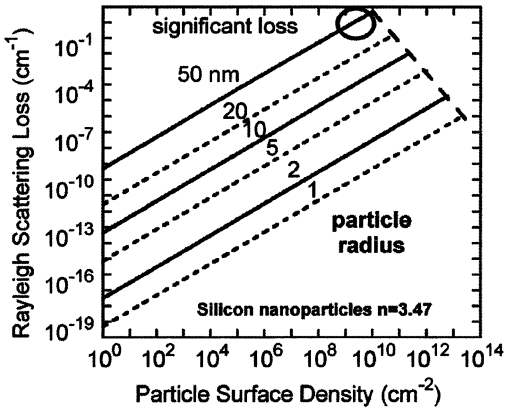

Fig. 10. Scattering loss due to high index particles bound to the surface. The in-plane lasers of the TLCS tolerate several cm^{-1} of scattering loss. Scattering from low-index particles such as proteins or polystyrene is negligible for all sizes and densities considered here.

the near infrared region is dominated by overtones of the mid-infrared absorption bands of C-H, O-H, and N-H bonds [21]. These overtones are weak, even in pure materials. In fact water, the most likely solvent for biochemical sensing, has stronger absorption than organics, amounting to $A = 3.2$ through a 1-cm path length. This corresponds to a loss $\alpha = 7.4\ \text{cm}^{-1}$. NIR absorption in alkanes is roughly half this value. Even if $\Gamma_{xy}\Gamma_z = 10^{-2}$, as in the case of a TLCS with a symmetrically clad sensing waveguide, the additional modal loss seen by the laser is less than 0.1 cm^{-1}. Proteins, and the alkane linker molecules commonly used to immobilize antibodies or nucleotides to surfaces also contain these absorbing bonds, but always at a lower density than in the pure solvents. We conclude that absorption loss will not be significant. One possible exception is if semiconducting nanoparticles or quantum dots are used for assay enhancement. In this case, the absorption edge of nanoparticle can be engineered to be remote from the sensor wavelength.

V. Summary

We have reviewed the experimental performance of the tunable laser cavity sensor, and analyzed the sensitivity to both bulk fluids and surface-bound species. From the experimental response, we predict that the asymmetrically clad waveguide design can detect changes in a bulk fluid index of $1 \cdot 10^{-4}$. While this is a respectable result for a device suitable for integration with microfluidics, we predict a hundred-fold improvement by changing the sensing waveguide to a symmetrically clad design. We have built a sensor using a self-aligned high-index-contrast symmetrically-clad waveguide, and have verified both the quantitative prediction and the feasibility of fabrication. To make use of the inherent sensitivity in field applications, it is necessary to improve the temperature stability of the sensor, either by better matching the operating points of the reference and sensing lasers, or by compensating the heterodyne signal drift through auxiliary on-chip measurements. With a predicted sensitivity of 150 femtograms in an affinity assay, the improved TLCS would be competitive with laboratory fluorescence techniques.

References

[1] S. Y. Rabbany, B. L. Donner, and F. S. Ligler, "Optical immunosensors," *Crit. Rev. Biomed. Eng.*, vol. 22, pp. 307–346, 1994.
[2] G. Ramsay, *Commercial Biosensors*. New York: Wiley, 1998.
[3] W. Lukosz, "Integrated optical chemical and direct biochemical sensors," *Sensors Actuators B*, vol. B29, pp. 37–70, 1995.
[4] K. M. Grace, K. Shrouf, S. Honkanen, P. Ayras, P. Katila, M. Leppihalme, R. G. Johnston, X. Yang, B. Swanson, and N. Peyghambarian, "Waveguide Zeeman interferometry for thin-film chemical sensors," *Electron. Lett.*, vol. 33, pp. 1651–1653, 1997.
[5] R. G. Heidemann and P. V. Lambeck, "Remote opto-chemical sensing with extreme sensitivity: Design, fabrication and performance of a pigtailed integrated optical phase-modulated Mach-Zehnder interferometer system," *Sensors Actuators B*, vol. B61, pp. 100–127, 1999.
[6] B. Maisenholder, H. P. Zappe, R. E. Kunz, M. Moser, and P. Riel, "Optical refractometry using a monolithically integrated Mach-Zehnder interferometer," presented at the 1997 Int. Conf. Solid-State Sensors Actuators, Chicago, IL, June 16–19, 1997.
[7] D. A. Cohen, E. J. Skogen, H. Marchand, and L. A. Coldren, "Monolithic chemical sensor using heterodyned sampled grating DBR lasers," *Electron. Lett.*, vol. 37, pp. 1358–1360, 2001.
[8] O. Hennig, Y. Beregovskii, R. Clemens, S. Mendes, M. Fallahi, and N. Peyghambarian, "Distributed Bragg reflector laser-based sensor for chemical detection," *Optics Commun.*, vol. 156, pp. 311–315, 1998.
[9] Y. Beregovski, O. Hennig, M. Fallahi, F. Guzman, R. Clemens, S. Mendes, and N. Peyghambarian, "Design and characteristics of DBR-laser-based environmental sensors," *Sensors Actuators B*, vol. B53, pp. 116–124, 1998.
[10] B. Mason, G. A. Fish, S. P. DenBaars, and L. A. Coldren, "Widely tunable sampled grating DBR laser with integrated electroabsorption modulator," *IEEE Photon. Technol. Lett.*, vol. 11, pp. 638–640, June 1999.
[11] Agility Communications (2003). [Online]. Available: www.agility.com
[12] L. A. Coldren and S. W. Corzine, *Diode Lasers and Photonic Integrated Circuits*. New York: Wiley, 1995. Appendix 3.
[13] O. Parriaux and G. J. Veldhuis, "Normalized analysis for the sensitivity optimization of integrated optical evanescent-wave sensors," *J. Lightwave Technol.*, vol. 16, pp. 573–582, Apr. 1998.
[14] M. Kerker, *The Scattering of Light*. New York: Academic, 1969, ch. 3.
[15] S. Kubitschko, J. Spinke, T. Bruckner, S. Pohl, and N. Oranth, "Sensitivity enhancement of optical immunosensors with nanoparticles," *Anal. Biochem.*, vol. 253, pp. 112–122, 1997.
[16] N. Matine, M. Dvorak, J. Pelouard, F. Pardo, and C. Bolognesi, "Fabrication and characterization of InP heterojunction bipolar transistors with emitter edges parallel to [001] and [010] crystal orientations," *Jpn. J. Appl. Phys.*, vol. 38, pp. 1200–1203, 1999.
[17] T. Asano, D. Feezell, R. Koda, M. H. M. Reddy, D. Buell, A. Huntington, E. Hall, S. Nakagawa, and L. Coldren, "InP-based all-epitaxial 1.3-μm VCSEL's with selectively etched AlInAs apertures and Sb-based DBRs," *IEEE Photon. Technol. Lett.*, vol. 15, pp. 1333–1335, Oct. 2003.
[18] B. Mason, J. Barton, G. Fish, and L. Coldren, "Design of sampled grating DBR lasers with integrated semiconductor optical amplifiers," *IEEE Photon. Technol. Lett.*, vol. 12, pp. 762–764, July 2000.
[19] S. Y. Rabbany, W. A. Marganski, A. W. Kusterbeck, and F. S. Ligler, "A membrane-based displacement flow immunoassay," *Biosensors Bioelectron.*, vol. 13, pp. 939–944, 1998.
[20] F. S. Ligler, B. P. Gaber, A. W. Kusterbeck, and G. A. Wemhoff, "Flow immunosensor method and apparatus," U.S. Patent 5 183 740, 1993.
[21] B. Osborne, "Near infrared spectroscopy in food analysis," in *Encyclopedia of Analytical Chemistry*, R. A. Meyers, Ed. New York: Wiley, 2000, vol. 5, pp. 4069–4082.

Daniel A. Cohen received the B.S. degree in physics, and the M.S. and Ph.D. degrees in electrical and computer engineering, all from the University of California, Santa Barbara, in 1984, 1994, and 1997, respectively.

He is currently a Principal Development Engineer at the University of California, Santa Barbara, after previous positions with Sloan Technology Corporation, Santa Barbara, California and the U.S. Army. He has published work on temperature compensation of diode lasers, wavelength tunable diode lasers, external cavity lasers for sensing applications, GaN optical properties and devices, and photonic integrated circuits for biochemical sensing.

Jill A. Nolde was born in St. Louis, MO, in 1977. She received the B.S. degree in electrical and computer engineering from Purdue University, West Lafayette, IN, in 1999, and the M.S. degree from the University of California, Santa Barbara in 2001, where she is currently working toward the Ph.D. degree in electrical and computer engineering.

She interned at Intel Corporation, the Massachusetts Institute of Technology,Cambridge, MA, and Nagoya University, Nagoya, Japan, before beginning study her Ph.D. studies. Her current research interests include widely tunable semiconductor lasers, integrated heterodyne receivers, and photonic integrated circuits for high sensitivity biosensing.

Anna Tauke Pedretti (S'02) was born in Dubuque, IA, in 1979. She received the B.S. degree from the University of Iowa, Iowa City, in 2001, and the M.S. degree from the University of California, Santa Barbara, in 2002, where she is currently working toward the Ph.D. degree in electrical and computer engineering from the.

Her current research interests focus on InP-based photonic integrated circuits for biosensor applications and widely tunable semiconductor lasers.

Chad S. Wang (S'99) was born in Racine, WI, in 1979. He received the B.S. degree from the University of Texas at Austin, in 2001, and the M.S. degree from the University of California, Santa Barbara, in 2002, where he is currently working toward the Ph.D. degree in electrical and computer engineering.

His current research interests focus on design and MBE growth of GaAs and arsenide compounds lattice-matched to InP for short and long-wavelength vertical-cavity lasers, respectively.

Erik J. Skogen was born in Minneapolis, MN in 1975. He received the B.S. degree from Iowa State University, Ames, in 1997, and the M.S. degree from the University of California, Santa Barbara, in 1999, where he is currently working toward the Ph.D. degree in electrical and computer engineering from.

His current research interests include widely tunable semiconductor lasers, monolithic integration for photonic integrated circuits, growth aspects in the InGaAsP material system using MOCVD, and quantum well intermixing.

Larry A. Coldren (S'6–M'72–SM'77–F'82) received the Ph.D. degree in electrical engineering from Stanford University, Stanford, CA, in 1972.

After 13 years in the research area at Bell Laboratories, Holmden, New Jersey, he was appointed Professor of Electrical and Computer Engineering at the University of California, Santa Barbara (UCSB), in 1984. In 1986, he assumed a joint appointment with Materials and ECE, and in 2000, the Fred Kavli Chair in Optoelectronics and Sensors. He is also Chairman and Chief Technology Officer of Agility Communications, Inc., Santa Barbara, CA. At UCSB, his efforts have included work on novel guided-wave and vertical-cavity modulators and lasers, as well as the underlying materials growth and fabrication technology. He is now investigating the integration of various optoelectronic devices, including optical amplifiers and modulators, tunable lasers, wavelength-converters, and surface-emitting lasers. He has authored or coauthored over 500 papers, five book chapters, one textbook, and has been issued 32 patents.

Dr. Coldren is a Fellow of the Optical Society of America, a past Vice-President of IEEE-LEOS, and has been active in technical meetings.